A Process for Shape Optimization of Filament Wound Pressure Vessels

Dr. Guclu Seber[1] and Dr. Myles L. Baker[2]
M4 Engineering, Inc., Signal Hill, CA, 90755

Kevin Roughen[3]
M4 Engineering, Inc., Signal Hill, CA, 90755

and

Joseph L. Griffin[4] and Matt H. Triplett[5]
U.S. Army Research, Development and Engineering Command, Redstone Arsenal, AL 35898

Nomenclature

L	=	pressure vessel cylinder length
r_o	=	polar radius
r_c	=	cylinder radius
r_m	=	local geodesic radius of curvature
w	=	tape width
α	=	winding angle
n	=	number of half circuits
N	=	number of circles
M	=	number of circuits
Z	=	axis of revolution
R	=	radial direction
L	=	longitudinal fiber direction
T	=	transverse fiber direction
$t_{helical}$	=	total thickness of helical windings at the cylinder
t_{hoop}	=	total thickness of hoop windings at the cylinder
E	=	Young's modulus of elasticity
G	=	shear modulus
ν	=	Poisson's ratio
σ	=	stress
ε	=	normal strain
γ	=	shear strain
FVR	=	fiber volume ratio
$S.F.$	=	safety factor
Q	=	orthogonal constitutive matrix
P	=	pressure
N_m	=	total axial force at a dome section
N_h	=	total circumferential force at a dome section
F_o	=	polar boss load
F_n	=	perturbation shape function
n_{pert}	=	number of total perturbations

[1] Senior Engineer, AIAA Member.
[2] President and CEO, AIAA Associate Fellow.
[3] Senior Engineer, AIAA Member.
[4] Senior Engineer, AIAA Member.
[5] Senior Engineer, AIAA Member.

I. Introduction

Filament wound composite pressure vessels are widely used in commercial and aerospace industries as high-pressure containers due to their high strength and lightweight. These vessels consist of a cylindrical body, domes at each end and occasionally an outer skirt structure around the cylindrical body, which provides additional strength as well as an attachment surface.

The commonly used 'wet' filament winding process is composed of four basic steps. First the dry filaments are impregnated with resin matrix by pulling them through a basin in a control fashion. These 'wet' filaments or tapes can then be accurately positioned onto the rotating mandrel surface by a delivery head. The CNC filament winding machines have several axes of motion, the number of which increases with the complexity of the winding pattern requirements. Winding patterns can involve helical, polar and hoop patterns.

Helical windings are laid at desired angles as the delivery head transverses back and forth while the mandrel is being rotated around its axis of rotation. Initially, the fibers are not adjacent to each other until additional circuits are transversed. This winding pattern results in crossovers that are believed to decrease the longitudinal strength. These windings are known to be non-slip for vessels with same polar openings at both ends.

In polar winding, the tapes run tangential to the polar opening at both ends and are laid adjacent to each other each. This makes polar winding a simple process, and particularly useful in spherical vessel applications.

Hoop windings are only applied to the cylindrical sections of closed end vessels at an angle of 90^o, whereas helical and polar windings can be used on both cylinders and domes. Hoop windings are used together with helical windings to produce a balanced-stress structure.

Once the filaments are wound on the mandrel, curing of the resin begins in the ovens. The cure process has a direct impact on the final quality of the pressure vessel, and therefore has to be done at well-defined temperatures and time periods. The final step involves the removal of the mandrel, which can be done by simply washing-away the soluble sand based mandrel or in other cases take advantage of collapsible or segmented mandrels.

For the filament wound composite pressure vessels, failure at the dome has been a significant problem. And, compared to other modes of failure, such as cylinder or skirt failure, dome failure is very undesirable as it introduces severe safety issues. In order to eliminate dome failure and design a structurally efficient vessel, considerable effort must be put towards analysis, shaping, material selection and fabrication of this region. In literature, experimental and analytical methods such as netting theory [3], orthotropic plate theory [1,2], have been used to achieve an optimum design for this region.

In this study, a finite element based shape optimization process has been introduced for designing filament wound pressure vessel mandrel counters with structural efficiency surpassing the classical geodesic shape historically considered to be optimal. The geodesic shape is well known from netting analysis to provide optimal structural efficiency and a non-slip filament winding pattern for theoretical domes for which the dome and cylinder interface effects are ignored. However, analytical and experimental test results [4,5] have demonstrated that these assumptions provide a limited representation of actual filament wound pressure vessel. The object of this study is to create an accurate finite element model of the filament wound pressure vessel to eliminate these limitations and provide a robust dome design achieved by a unique shape optimization process.

II. Theoretical Considerations

A. Geodesic Winding Pattern

The geodesic winding pattern is considered to be very efficient in filament wound pressure vessels resulting in a constant stress (isotensoid) distribution and a non-slip condition for the fibers. Mathematically stated, it corresponds to a curve, which connects two points on the shortest way within a warped surface. Equation (1) describes a

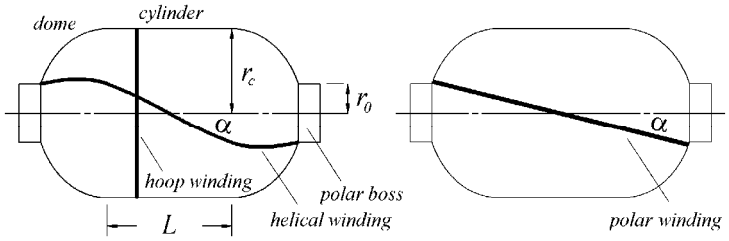

Figure 1: Types of winding and geometric parameters for composite pressure vessels.

geodesic curve for a filament wound pressure vessel.

$$r\sin(\alpha) = constant \tag{1}$$

where α is the winding angle between a filament and a meridian line at a point on the surface, and r is the radial distance measured with respect to the axis of rotation, Z.

The constant in Eq. (1) can be determined by applying a tangency condition at the polar opening, i.e. at $r=r_o$, $\alpha=\pi/2$. Equation (1) then becomes

$$\sin(\alpha) = \frac{r_o}{r} \tag{2}$$

The mathematical expression for a geodesic dome contour can be obtained using the force equilibrium. For a filament wound pressure vessel only composed of helical fibers (with $\pm\alpha$ as the winding angle), Eqs. (3a-b) show the axial and circumfrential forces per unit circumference at the cylinder, calculated using netting theory, i.e. filaments carry all the loads, matrix effects are ignored.

$$N_m = t_f \sigma_f \cos^2\alpha = \frac{\mathrm{Pr}_c}{2},\ N_h = t_f \sigma_f \sin^2\alpha = \mathrm{Pr}_c \tag{3a-b}$$

where σ_f and t_f. are the constant allowable filament stress and local fiber thickness, respectively, and P is the pressure.

Using the notation introduced in Fig. 2, another set of force equilibrium equations can be written at the dome as shown in Eqs. (4a-b).

$$N_m = \frac{Pr}{2cos\psi},\ \frac{N_m}{r_m} + \frac{N_h}{r}\cos\psi = P \tag{4a-b}$$

By using Eqs. (3a-b), the following ratio can be obtained between the circumfrential and axial load.

$$\frac{N_h}{N_m} = \tan^2\alpha \tag{5}$$

Substituting Eqs. (4a) and (5) into Eq. (4b), and solving for r_m we get

$$r_m = \frac{r}{\cos\psi(2-\tan^2\alpha)} \tag{6}$$

Equation (6) can be solved by applying increments of ψ with the help of Eqs. (7a-b) and (8a-c).

$$\Delta r = -r_m \Delta\psi \sin\psi,\ \Delta z = r_m \Delta\psi \cos\psi \tag{7a-b}$$

$$\psi = \sum \Delta\psi,\ r = r_c + \sum \Delta r,\ z = z_c + \sum \Delta z \tag{8a-c}$$

One must note that Eq. (6) is not defined for $r \le 1.22r_o$ due to an inflection point that occurs at $\alpha=54^o$. In practice, a polar boss of conical or spherical shape with radius $\ge 1.22r_o$ is inserted to this opening for the winding process to take place.

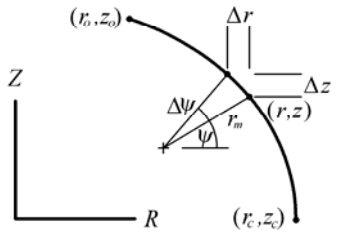

Figure 2: Notation for the geodesic winding pattern at the dome.

Assuming that the tow width is small compared to the radius of the case, an approximate thickness distribution can be computed that is accurate over most of the pressure vessel, except for the polar regions. Figure 3 shows the basic geometry of the filament winding process, and represents an axisymmetric section of the pressure vessel. At the local point in question, the tape makes an angle α with respect to the local meridian line. This results in an effective tape width of $w/\cos\alpha$ in the circumferential direction. Since the total circumference is $2\pi r$, the equivalent average thickness of a single tape band can be expressed as

$$t_{average} = \frac{wt}{2\pi r \cos\alpha} \tag{9}$$

This results in the following relationship for the thickness distribution

$$\overline{t} = \frac{nA}{2\pi\cos\alpha} = \frac{nA}{2\pi\sqrt{r^2 - r_0^2}} \tag{10}$$

where A is the cross-sectional area of the wrapping band, and n is the number of half-circuits (pole-to-pole paths) of the helical winding.

One of the largest problems with helical winding is identifying "good" winding schedules. This is a challenge because it is easy to define winding schedules that do not provide uniform coverage of the entire pressure vessel. While there may be enough total material, due to the intricacies of the winding pattern, the material may not be evenly distributed, but may leave large gaps in the coverage of the cylinder. This leads to a constraint on the winding schedule; it must be "good".

It takes some thought to express this constraint in mathematical terms. Essentially the winding schedule must be such that the helical windings repeat themselves with an offset of one tape width. This implies that the tows will (after winding is complete) will lie exactly next to one another. If we define N to be the number of helical circuits

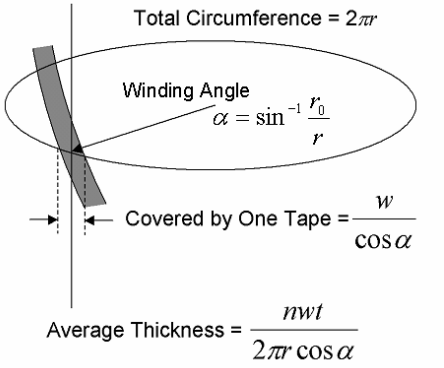

Figure 3: Geometry of filament winding process.

made before the pattern begins to repeat itself, this implies that after N circuits, the helical winding must wind around the mandrel by some number of complete revolutions, plus a small amount to account for the additional tape width. Defining M to be the number of circles covered in N circuits of winding, the following mathematical equations can be derived.

$$N\Delta\theta\left(r, r_o, w, l, \alpha\right) = 2M\pi + \frac{w}{r\cos\alpha} \tag{11}$$

$$\Delta\theta \approx \frac{2l}{r}\tan\alpha + 4\cos^{-1}\frac{r_o + w/2}{r} \tag{12}$$

$$w = \frac{2\pi r\cos\alpha}{NN_2} \tag{13}$$

where w represents the tape width, N_2 is the number of repetitions. Eq. (12) represents the total angle ($\Delta\theta$) covered by one helical winding. The version of the equation shown here is based on the implementation of the COBSTRAN code [], and has several approximations included. See Ref. [] for details.

Equations (11-13) define a nonlinear set. Solution of this set starts with a basic case geometry (length, radius), a nominal tape width (called w_0, and used to start the iteration), and the two integer parameters N and M. Iterating to solve the set of nonlinear equations results in the actual tape width required, the pole radius, and the winding angle. This effectively limits the infinite number of possible windings (as defined by any value of the winding angle) to a smaller number of "good" windings (as defined by the integer values of M and N). This ensures that only "good" winding schedules that will uniformly cover the entire motor case are analyzed in detail.

A challenge in validating this approach to limiting the possible winding schedules to "good" helical windings has been in the sensitivity of the results to small modifications in the geometry. An example of this sensitivity is shown in Figure 4, which shows the results of a filament winding simulation using slightly different values of the pole radius and the winding angle. These small changes in the winding parameters have a large impact on the resulting winding quality. In the left half of Figure 4, a "good" result is shown, with a winding angle of 15.95 degrees. Note that for a single pass of helical windings, two plies have been generated for each node around the circumference. The right half of the figure shows a "bad" result, where the winding angle has been changed to 15.46 degrees. This results in a winding that has very thick lay-ups in some areas of the case, but large areas that have no coverage at all. This illustrates the importance of limiting the optimization to windings that provide uniform coverage. A large number of significant figures (at least 6-8) are required to generate acceptable accuracy.

B. Preliminary Optimization of the Baseline Pressure Vessel

The initial sizing of the baseline pressure vessels is done using a new software tool [6] that performs a preliminary optimization process based on the basic netting theory and ideal geodesic winding assumptions. For the process to initialize, the required input includes the basic geometric parameters such as the case length and radius, allowable polar radius range and tape width, material selections from a database for both helical and hoop plies and the pressure applied to the vessel.

During optimization, several winding patterns are evaluated by iteratively varying the polar radius and the tape width to achieve uniform coverage of the mandrel surface as discussed in the previous section. Windings that do not provide uniform coverage and are not physically possible are eliminated, i.e. too many filament crossovers and bold spots on the surface or calculated polar radius is not within the allowable range.

Among the possible winding patterns, the one with the lowest structural weight is selected as the optimum design. The results of the optimization process, i.e. polar radius, nominal tape width, total hoop and helical ply thicknesses, number of circles and circuits are used to create the 'baseline' finite element model discussed in the following section.

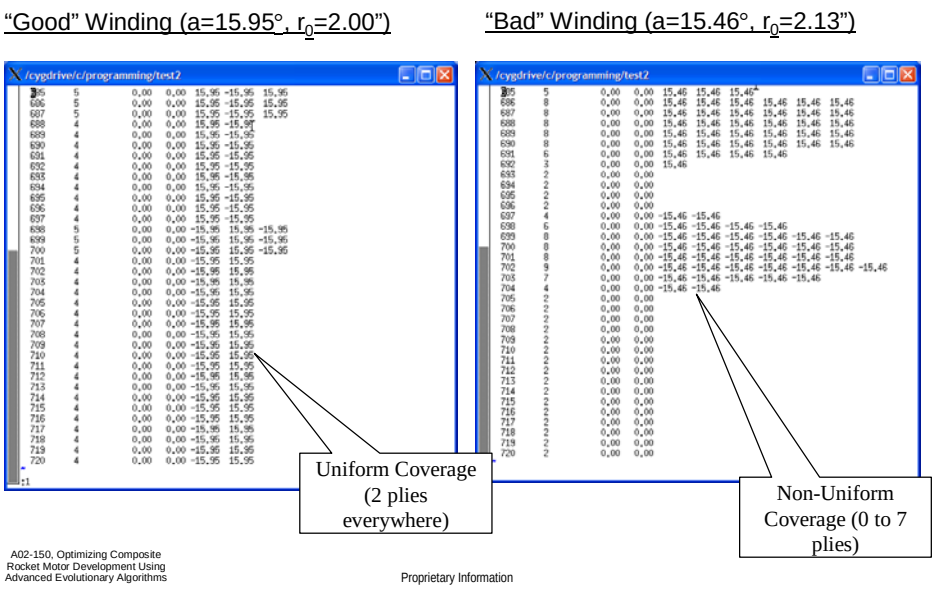

Figure 4: Example of "Good" and "Bad" Winding Schedules and Sensitivity on Input Parameters.

C. The Finite Element Model

For dome shape optimization of filament wound pressure vessels, axisymmetric ABAQUS Finite Element models are created to accurately represent the geometry and stiffness at the dome, cylinder, and the transition regions by the same software tool [6] that also performs the preliminary optimization. By taking advantage of the symmetry, only half of the structure is modeled with the appropriate boundary conditions. The tasks involved in creating baseline finite element models include mesh generation, calculation of hoop and helical ply properties, applying forces and boundary conditions and estimating fiber stresses by postprocessing the results obtained. Each of these tasks will be discussed in detail in the upcoming sections.

The mesh associated to the filament wound pressure vessel is generated automatically according to the parameters supplied by the user. These parameters mainly control the density of the mesh in both axial and radial directions. User also has control over the size of the hoop ply drop-off region to model vessels with different manufacturing features.

This mesh employs 4-node bilinear solid axisymmetric elements with incompatible modes known as CAX4I in ABAQUS. In the hoop ply drop-off region at the dome cylinder interface, 3-node linear elements (CAX3) are employed to provide continuity in the mesh by filling up the triangular gaps. Both types of elements have 2 degrees-of-freedom per node, i.e. displacements U_R *and* U_Z in radial and axial directions, respectively.

During mesh generation, the geodesic mandrel is used as a reference surface and layers of elements are stacked in a direction perpendicular to it. This approach results in a uniform mesh that can be deformed smoothly for the purposes of shape optimization.

In finite element models created, plies of helical and hoop windings are grouped into layers of elements to represent the winding pattern of the pressure vessel. The orthotropic properties for these elements are calculated considering the winding angle and type of material being used. Here, the variation in the winding angle is assumed to be constant along the thickness. The details of orthotropic property calculations are discussed in the following section on classical lamination theory.

Manufacturing details at the cylinder to dome transition are represented by the finite elements that blends layers of cylindrical region hoop plies into the helical plies at the dome-cylinder interface to characterize the effect of the hoop ply drop-off. See Figure 5 for details. For composite pressure vessels, it is known that cylindrical hoop plies slightly extend to the dome region as a result of the manufacturing process. In this finite element model, this is taken into account and the size of the region can be adjusted by the user.

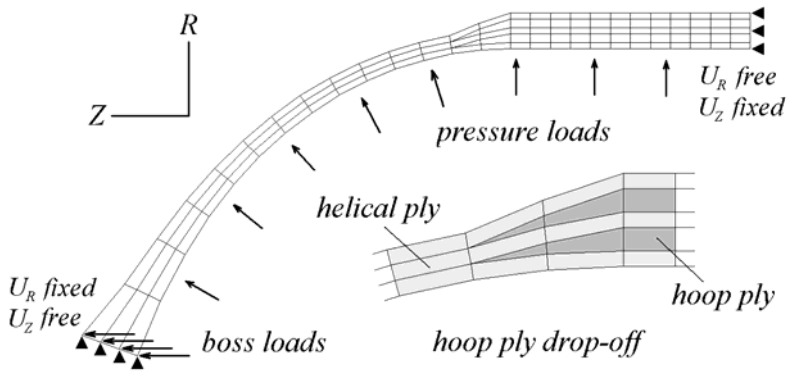

Figure 5: ABAQUS Finite Element model of a filament wound pressure vessel.

Boundary conditions applied to this finite element model reflect the symmetry in the structure. At the dome end of the model, axial displacement is free to allow for the expansion of the vessel, whereas the radial one is fixed due to presence of the solid polar boss. At the cylinder midpoint, the axial displacement is fixed and the radial one is free. This selection of boundary conditions avoids singularities due to unconstrained rigid body translations/rotations and does not over-constrain the system. See Figure 5.

In order to compensate for pressure acting on the polar boss, which is not modeled in this study, an equivalent circumferential load is applied to the dome end. This force can be calculated as shown in Eq. (14) and must be distributed onto dome nodes as point loads with equal magnitudes acting along the axis of revolution pointing outside, away from the polar opening. Ignoring these force results in erroneous results and leads to a force unbalance in the model and an unrealistic curling of the dome region inwards. The effects of pressure acting on the rest of the structure can directly be applied to the finite element model as shown in Figure 5.

$$F_o = 2\pi(1.22r_o)P \tag{14}$$

D. Classical Lamination Theory

The filament wound pressure vessels are shell structures constructed from symmetrical laminae that result in orthotropic layers. In this study, each axisymmetric element used in the finite element model is assumed to have orthotropic properties, which can be calculated by averaging the directional properties associated to fibers that run in $\pm\alpha$ directions with respect to meridian lines and the matrix surrounding them. In order to calculate these properties, classical lamination theory will be employed [].

Figure 6 shows a typical laminate geometry. *L-T* coordinate system is associated to the fibers in longitudinal and transverse directions. The engineering constants of a fiber-matrix composite can be determined using the data provided by the manufacturers and the fiber volume ratio (FVR) used in the mix. In these composites, matrix surrounds and holds the fibers together and provides the transverse stiffness. The longitudinal properties are dominated by the strength provided by the fibers, which are somewhat lowered by the presence of the matrix. In typical filament wound pressure vessels, the FVR is about 55%. The engineering constants associated to the composite material can be used to calculate the constitutive matrix *Q* that relates strains to stresses as shown in Eqs. (15-21).

$$Q_{11}^{'} = \left(1 - v_{23}^2 E_{33}/E_{22}\right)\frac{E_{11}}{V} \tag{15}$$

$$Q_{12}^{'} = \left(v_{12} + v_{13}v_{23} E_{33}/E_{22}\right)\frac{E_{22}}{V} \tag{16}$$

$$Q_{13}^{'} = \left(v_{12} + v_{12}v_{23}\right)\frac{E_{33}}{V} \tag{17}$$

$$Q_{22}^{'} = \left(1 - v_{13}^{2}\, E_{33}/E_{11}\right)\frac{E_{22}}{V} \tag{18}$$

$$Q_{33}^{'} = \left(1 - v_{12}^{2}\, E_{22}/E_{11}\right)\frac{E_{33}}{V} \tag{19}$$

$$Q_{44}^{'} = G_{23}\,,\ Q_{55}^{'} = G_{13}\,,\ Q_{66}^{'} = G_{12} \tag{20}$$

$$V = 1 - v_{12}(v_{12}E_{22}/E_{11} + 2v_{23}v_{13}E_{33}/E_{11}) - v_{13}^{2}E_{33}/E_{11} - v_{23}^{2}E_{33}/E_{22} \tag{21}$$

In order to obtain the ply properties used in the finite element calculations, the constitutive matrices for the equal number of laminae with fibers running along + and - α directions with respect to the element coordinate system must be transformed and averaged. This results in the orthotropic constitutive matrix as shown in Eqs. (22-30).

$$Q_{11} = Q_{11}^{'}m^{4} + 2m^{2}n^{2}(Q_{12}^{'} + 2Q_{66}^{'}) + Q_{22}^{'}n^{4} \tag{22}$$

$$Q_{12} = m^{2}n^{2}(Q_{11}^{'} + Q_{22}^{'} - 4Q_{66}^{'}) + Q_{11}^{'}(m^{4} + n^{4}) \tag{23}$$

$$Q_{13} = Q_{13}^{'}m^{2} + Q_{23}^{'}n^{2} \tag{24}$$

$$Q_{22} = Q_{11}^{'}n^{4} + 2m^{2}n^{2}(Q_{12}^{'} + 2Q_{66}^{'}) + Q_{22}^{'}m^{4} \tag{25}$$

$$Q_{23} = Q_{13}^{'}n^{2} + Q_{23}^{'}m^{2} \tag{26}$$

$$Q_{33} = Q_{33}^{'} \tag{27}$$

$$Q_{44} = Q_{44}^{'}m^{2} + Q_{55}^{'}n^{2} \tag{28}$$

$$Q_{55} = Q_{44}^{'}n^{2} + Q_{55}^{'}m^{2} \tag{29}$$

$$Q_{66} = m^2 n^2 (Q_{11}^{'} + Q_{22}^{'} - 2Q_{12}^{'}) + Q_{66}^{'} (m^2 - n^2)^2 \tag{30}$$

where $m = \cos(\alpha)$, $n = \sin(\alpha)$ with α being the positive winding angle. The non-listed elements of the constitutive matrix are simply zero.

The 9 nonzero components of the orthogonal constitutive matrix can then be incorporated into the ABAQUS finite element model along with the orientation angle with respect to *R-Z* coordinate system, which can be determined from the element nodal coordinates as explained in the previous sections.

E. Stress Recovery for the Fibers

In order to recover the fiber stresses, the results obtained using the axisymmetric finite element model require postprocessing. The default stress values obtained from the finite element solution simply present the results in the element coordinate systems for the average orthotropic properties calculated. Transforming these stresses into the *L-T* coordinate system directly will be erroneous due to loss of information caused by the averaging of symmetric plies.

By using the stress strain relations, the fiber stresses can be determined correctly. In this process, the first step is to acquire the element strains from the ABAQUS finite element solution. The strains can be transformed into the fiber coordinate system L-T as shown in Eqs. (). One must note that the shear strain γ_{13} is equal to zero for axisymmetric formulation but is included for the sake of completeness in the derivations.

$$\{\varepsilon\}_{L-T} = [T_\varepsilon]\{\varepsilon\}_{1-3} \tag{31}$$

$$\{\varepsilon\}_{L-T} = \lfloor \varepsilon_L \quad \varepsilon_T \quad \gamma_{LT} \rfloor \tag{32}$$

$$\{\varepsilon\}_{1-3} = \lfloor \varepsilon_1 \quad \varepsilon_3 \quad \gamma_{13} \rfloor \tag{33}$$

$$[T_\varepsilon] = \begin{bmatrix} m^2 & n^2 & -mn \\ n^2 & m^2 & mn \\ 2mn & -2mn & m^2 - n^2 \end{bmatrix} \tag{34}$$

By using the fiber strains and stress-strain relations in 2D, the fiber stress can be calculated as shown in Eq. (35). The maximum fiber stress in the helical dome fibers determines the value of the objective function during optimization.

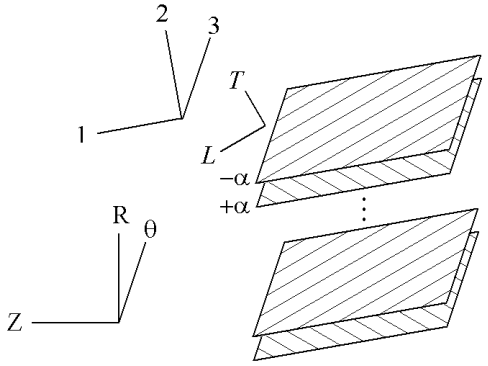

Figure 6: Laminate geometry for filament wound pressure vessels.

$$\sigma_L = Q_{11}\varepsilon_L + Q_{12}\varepsilon_T + Q_{66}\varepsilon_{LT} \tag{35}$$

F. Shape Optimization Process

As presented in the following section, the finite element analysis performed on the baseline model shows stress concentrations for helical fibers in the hoop ply drop-off region at the dome-cylinder interface. These concentrations are due to high bending type forces resulting from the change of total winding thickness and local radius of curvature as helical and hoop plies blend into each other.

By reshaping the dome contour and in effect changing the local radii of curvature, bending forces acting at the dome can be eliminated. This creates a more efficient load path and results in a more uniform stress distribution for the fibers, thus increasing the load carrying capacity of the pressure vessel.

The shape optimization process illustrated in Fig. 7 can be used to reshape the dome surface. As one can see, the shape optimization starts with a baseline model, created using the initial optimization process discussed earlier. From this baseline model, several perturbed models can be created. These models consist of shifted nodal points, coordinates of which are calculated from the baseline model by using appropriate shape functions to represent the perturbations. Eq. (36) shows the shape functions used to create the perturbed models.

$$F_n(s) = 1 - \cos\left(\frac{2\pi(s - s_{n-1})}{s_{n+1} - s_{n-1}}\right),\ s_n \le s < s_{n+1} \tag{36}$$

$$F_n(s) = 2.,\ s < s_n \tag{37}$$

$$s_{n-1} = (n-1)\Delta s,\ s_n = n\Delta s,\ s_{n+1} = (n+1)\Delta s,\ \Delta s = s_{total} / n_{pert},\ n = 0,1,2... < n_{pert} \tag{38a-c}$$

where s, n_{pert} and s_{total} are the distance measured from the polar opening, the total number of perturbations, the total length of the dome section, respectively.

The number of perturbed models used in the shape optimization process also determines the number of design variables present. During optimization, each design variable introduces a small amount of perturbation to the baseline model nodal coordinates, which is in direct proportion with the scale used to create perturbed models and the magnitude of the design variable itself. The nodal coordinates of the baseline model are in effect displaced locally according to the shape function along a direction perpendicular to the mandrel surface, see Figure 7.This results in well-behaving finite element meshes for the trial models.

Once the nodal coordinates of the trial model are created, the lamina properties are updated using the geodesic equations and element connectivities, material properties, boundary conditions and forces are applied by using the baseline model as a reference.

The ABAQUS solution obtained from the axisymmetric trial model provides displacements, strains and stresses. As discussed in the previous section, postprocessing of this data provides the stresses in helical fibers of the dome region, the maximum of which provides the value of the objective function.

The optimizers selected for this study comes from the SciPy library [] that is readily available. In this library, several gradient-based methods are available as well as genetic algorithms. It has been observed that genetic algorithms were very useful in determining a good starting point for the gradient-based methods that follow them for further improvement of the results. During the second stage gradient-based optimization, modified Powell method [] is used successfully for the configurations tested. In addition, Nelder-Mead Simplex algorithm [] is also employed with similar success.

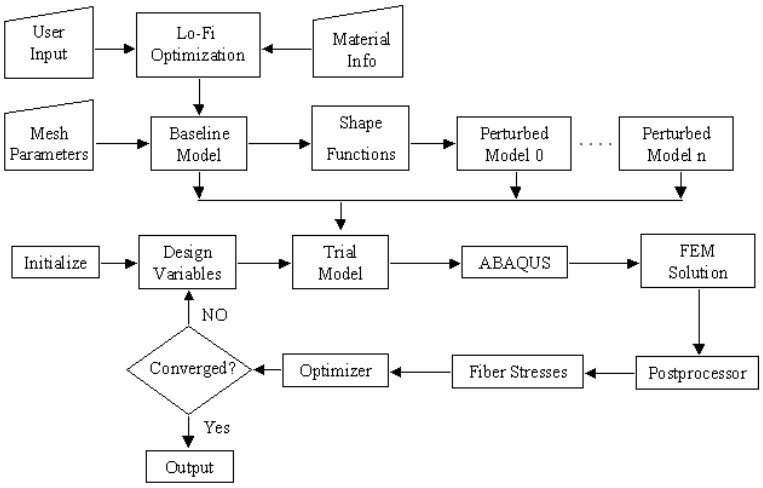

Figure 7: Flow chart for the shape optimization process.

III. Results and Discussion

A. Baseline Model

For the baseline model, a generic pressure vessel with the following properties is designed using the Motor Case Design Software. A preliminary design process was implemented in order to calculate the hoop and helical ply thicknesses of the cylinder and the polar radius in order to satisfy the strength and geodesic filament winding criteria, respectively.

$L = 10$ in.

$r_C = 8.0$ in.

$r_O = 3.1215$ in.

$t_{helical} = 0.1463$ in.

$t_{hoop} = 0.1001$ in.

$P = 5500$ psi.

$S.F. = 1.5$

helical and hoop materials = *T1000 series fibers* mixed with resin at 60% FVR

Figure 4 presents the fiber stresses obtained for this model. The stress concentration in the dome cylinder interface is clearly present for this model for which the stress peaks by a factor of 1.6 as compared to the theoretical uniform geodesic stress distribution.

B. Optimized Model

The shape optimization process employed significantly (about 30%) reduced the peak stresses in the optimized model as shown in Figure 9, when compared to the baseline model that employs the classical geodesic dome shape (see Figure 8). A total of 5 design variables (perturbed models) were used in this study. In shape optimized model, bending load at the transition region was eliminated. This can be observed by comparing the deformations of the baseline and optimized models, which are dominated by bending and axial type motions, respectively, as illustrated in Figure 10. One can note that dome contour of the optimized model is only slightly different from the baseline, which can easily be reflected to the fabrication process.

C. Experimental Results

In order to validate our results, we are currently fabricating 6 baseline bottles and 6 optimized bottles to be tested using hydro-burst pressure methods.

IV. Conclusion

1. The ABAQUS finite element models are capable of accurately predicting behavior of filament wound composite vessels including the dome stress concentration.
2. The dome shape optimization process has been observed to be an effective tool in improving the strength of filament wound composite vessels by effectively removing residual bending stresses at the ply drop-off.
3. Careful selection of smooth and continuous shape functions to create perturbed models is crucial in achieving convergence in dome shape optimization.
4. In dome shape optimization genetic algorithms have been very effective in reducing the maximum fiber stress. The gradient-based methods were observed to show faster convergence, with stress reduction capabilities comparable to genetic algorithms.

Acknowledgments

This research was funded under U.S Army SBIR project A02-150 Phase II, with Joseph Griffin as the project monitor.

References

[1]Liang, C., Chen, H., and Wang., C., "Optimum Design of Dome Contour for Filament-Wound Composite Pressure Vessels Based on a Shape Factor," *Composite Structures*, Vol. 58, 2002, pp. 469-482.

[2]Fukunaga, H., Uemura, M., "Optimum Design of Helically Wound Composite Pressure Vessels," *Composite Structures*, Vol. 1, 1983, pp. 31-49.

[3] Peters, S. T., Humphrey, W. D., and Foral, R. F., *Filament Winding Composite Structure Fabrication*, 2nd ed., SAMPE Publications, California.

[4]Baker, M. L., Gondouin, A., "SBIR Topic A02-150 Phase I Interim Report," 2004.

[5]Baker, M. L., Seber, G., "SBIR Topic A02-150 Phase II Interim Report," 2005.

[6]MCD, Motor Case Design Software, Ver. 1.2, M4 Engineering, Inc., Signal Hill, CA, 2005.

[7]Whitney, J. M., *Structural Analysis of Laminated Anisotropic Plates*, 1st ed., Technomic Publishing, Pennysylvania.

[8]Oliphant, T., Jones, E., Peterson, P., SciPy: Open source scientific tools for Python, http://www.scipy.org/, 2006

[9]Cobstran, Ver. 4.1, Alpha Star Corporation, 5199 E PCH, #410, Long Beach, CA, 2005.

[10]Nelder, J. A. and Mead, R. "A Simplex Method for Function Minimization." Comput. J. 7, 308-313, 1965.

[11]Powell, M.J.D., "An Efficient Method for Finding the Minimum of a Function of Several Variables Without Calculating Derivatives," Comp. J. 7, 155-162, 1964.

[12]Powell, M.J.D., "Nonconvex Minimization Calculations and the Conjugate Gradient Method," Lecture Notes in Mathematics, Vol. 1066, pp. 122-141, 1984.

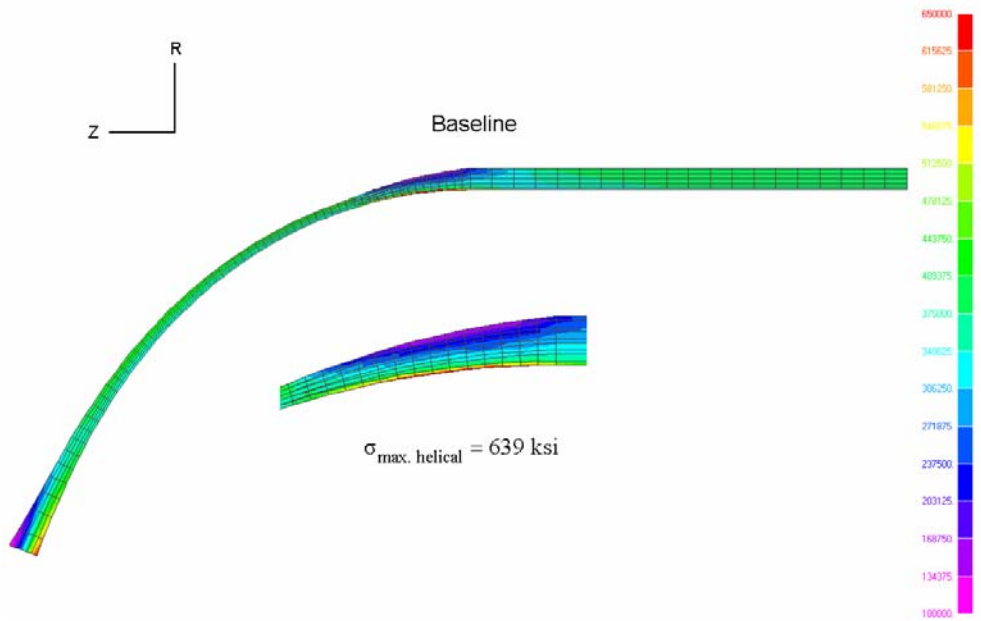

Figure 8: Stress concentration at the dome/cylinder transition for the baseline model.

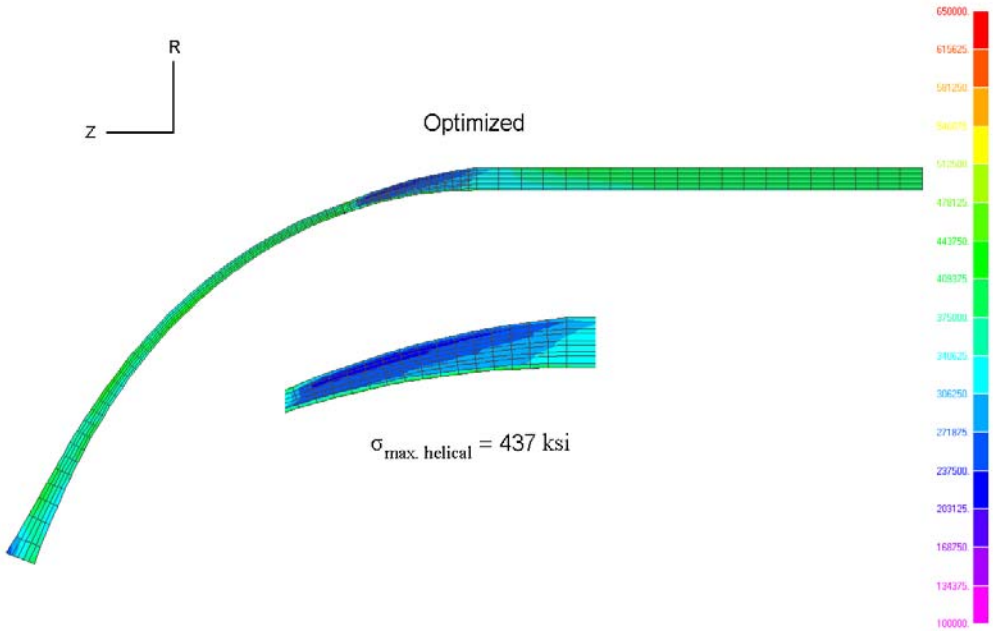

Figure 9: Shape optimized filament wound pressure vessel.

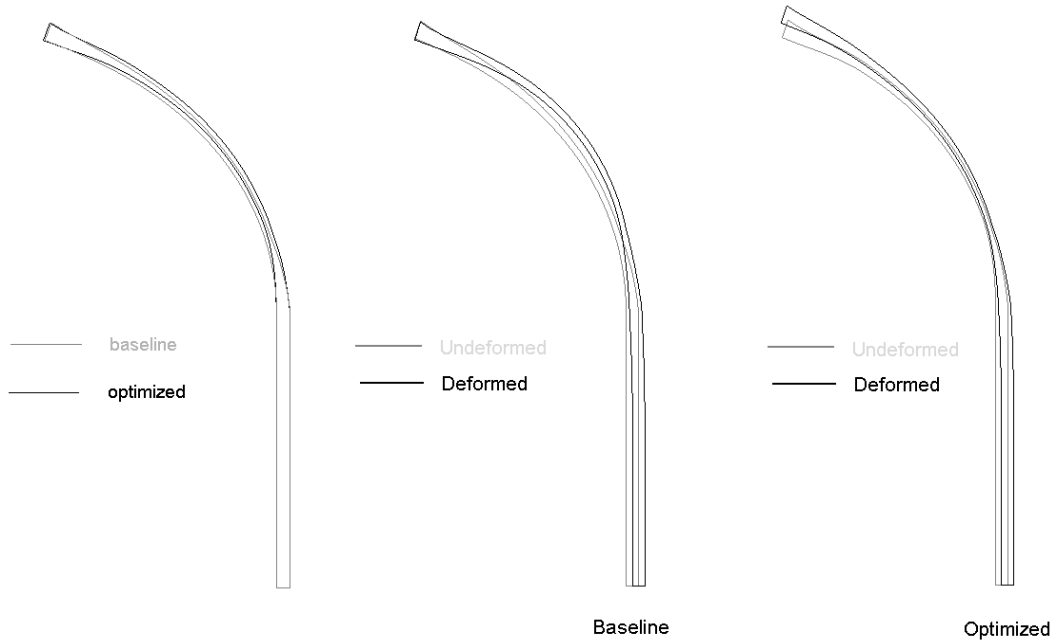

Figure 10: Contour comparison and deformation modes for the baseline and optimized pressure vessels